Transportation Research Part C 128 (2021) 103110

Contents lists available at ScienceDirect

Transportation Research Part C

journal homepage: www.elsevier.com/locate/trc

Robust traffic wave damping via shared control☆

Jingjing Jiang [a,*], Alessandro Astolfi [b,c,d], Thomas Parisini [b,e]

[a] Dept. of Aeronautical and Automotive Engineering, Loughborough University, LE11 3TU, UK
[b] Dept. of Electrical and Electronic Engineering, Imperial College London, London, SW7 2AZ, UK
[c] the KIOS Research and Innovation Center of Excellence, University of Cyprus, Cyprus
[d] DICII, University of Roma "Tor Vergata", Via del Politecnico 1, 00133 Rome, Italy
[e] Dept. of Engineering and Architecture at University of Trieste, Italy

ARTICLE INFO

Keywords:
Traffic wave damping
Shared control
Congestion mitigation
Robust control
Human driver instantaneous satisfaction index

ABSTRACT

The traffic wave damping problem in a circular single lane track is addressed and solved via a shared control technique which takes a model of the human drivers' driving habits into consideration. A formal analysis shows that the effectiveness of the proposed shared controller does not depend on the parameters of the human driver's model, which is an important property in the implementation of the shared controller, since these parameters are difficult to measure, and vary from one human driver to another and from one driving situation to another. In addition, the proposed control law is robust: the stop-and-go wave can be dampened and there is no collisions among vehicles even if there is noise on the information each vehicle receives from the higher level traffic control center. A comparison between performances of the vehicles with and without the proposed control scheme demonstrates the robustness and the effectiveness of the shared control solution.

1. Introduction

Traffic waves, also known as stop-and-go waves, phantom jams and ghost jams, are caused by the instability of the system describing the dynamics of traffic flow on highways: slight disturbances in the distribution of cars on the highway are amplified when the density of the highway is higher than a certain value and finally generate traffic waves (Peng et al., 2011; Wilson, 2008; Orosz et al., 2009). The most common causes for the occurrence of traffic waves is lane changing maneuvers (Laval and Daganzo, 2006; Ahn et al., 2007; Laval, 2005). However, recent researches have shown that the waves could also be generated without lane changes or any other types of bottlenecks, such as traffic accidents and sharp curves (Orosz et al., 2008; Tadaki et al., 2013; Laval and Leclercq, 2010). Such a phenomenon is experimentally reproducible, as demonstrated in (Sugiyama et al., 2008; Stern et al., 2018), and has significant negative impacts on traffic, resulting in extra energy consumption and emission, additional travelling time and loss of driving comfort (Laval and Leclercq, 2010; Barth and Boriboonsomsin, 2008). Even worse, it increases driving hazards (Marchesini and Weijermars, 2010; Wang et al., 2009).

To relieve the nuisance caused by traffic waves, several studies on the formation and propagation of waves, both at the microscopic

☆ This work has been partially supported by the European Union's Horizon 2020 research and innovation programme under grant agreement No 739551 (KIOS CoE), and by the Italian Ministry of Research in the framework of 2017 program for Research Projects of National Interest (PRIN), Grant no. 2017YKXYXJ.

* Corresponding author.
E-mail addresses: J.Jiang2@lboro.ac.uk (J. Jiang), a.astolfi@imperial.ac.uk (A. Astolfi), t.parisini@gmail.com (T. Parisini).

https://doi.org/10.1016/j.trc.2021.103110
Received 10 May 2019; Received in revised form 13 March 2021; Accepted 24 March 2021

Nomenclature

T_s	sampling time $[s]$
n_c	number of feedback delay samples, *i.e.* the measurement delay of the feedback controller is $T_c = n_c T_s$
n_d	human driver's reaction delay sample, *i.e.* human driver's reaction time T_d is calculated as $T_d = T_s n_d$
a_{h_i}	acceleration of Vehicle i generated by the human driver $[m/s^2]$
a_{c_i}	acceleration of Vehicle i generated by the feedback controller $[m/s^2]$
a_{s_i}	acceleration of Vehicle i generated by the shared-controller $[m/s^2]$
a^i_{min}	minimum acceleration of Vehicle i $[m/s^2]$
a^i_{max}	maximum acceleration of Vehicle i $[m/s^2]$
v^i_{max}	maximum speed of Vehicle i $[m/s]$
v^r	recommended speed from the higher-level traffic control center $[m/s]$
d_{min}	minimum distance between two vehicles to avoid collisions $[m]$
$d_{i,j}(k)$	distance between Vehicle i and Vehicle j at the time instant kT_s $[m]$
$f_i(k)$	value of the sharing function for Vehicle i at the time instant kT_s
$\mathscr{S}_i(k)$	instantaneous satisfaction index for the human driver of Vehicle i
δ_i	communication disturbance or fault for Vehicle i $[m/s]$

level (Daganzo, 1994; Treiber et al., 2006; Yeo and Skabardonis, 2009) and at the macroscopic level (Flynn et al., 2009; Flynn et al., 2009), have been carried out. One popular solution to the occurrence of traffic waves is obtained by controlling the density of the highways by Ramp Metering (RM) control (Papamichail et al., 2010; Gomes and Horowitz, 2006), while another widely used method is Variable Speed Limits (VSL) control (Papageorgiou et al., 2008; Hegyi et al., 2008). A combination of RM and VSL control has been proposed for instance in (Carlson et al., 2010; Hou et al., 2007; Carlson et al., 2014). In order to achieve RM control and VSL control, various control methods have been implemented, such as for example cascade control (Carlson et al., 2011), Model Predictive Control (Hegyi et al., 2005), the use of autonomous vehicles (Guo and Wang, 2019; Guo and Li, 2019; Guo and Li, 2019) and Iterative Learning Control (Hou et al., 2007).

In particular, the paper (Stern et al., 2018) has shown that traffic waves are significantly reduced with the help of a small number of autonomous vehicles on the freeway. Even though autonomous vehicles have several benefits, they may harm passengers' experience: to improve the efficiency of the overall transportation system, the vehicle may move slowly or even stop when nothing ahead impedes its journey.

This paper solves the traffic wave damping problem via a shared control (Abbink et al., 2018; Jiang et al., 2016) algorithm, that is, it provides an algorithm which relies on the integration of the human driver and a feedback controller. Such a shared-control law aims at improving the traffic efficiency without dissatisfying the human driver and the passengers.

Furthermore, the control action generated by the feedback controller depends on the information sent by the higher level traffic control center. In reality, such information may be affected by noise. Or, even worse, the information may be faulty. Therefore, it is important that the proposed controller be sufficiently robust to deal with these issues.

The main contributions of the paper are stated as follows. A novel driving assistant controller, which is able to damp the stop-and-go wave phenomenon in a single-lane circular freeway (the benchmark in (Stern et al., 2018)) without making human driver dissatisfied, is proposed. We assume that a traffic control center, which sends information and recommended actions to all the vehicles in the lane, is available. The proposed control design is not based on parameter values representing the human driver's behaviour. In other words, the established shared controller is independent from the specific features describing the behaviour of the human drivers and from the driving situation. In addition, the proposed control scheme is robust to communication noise and faults. A theoretical analysis showing the effectiveness and the robustness of the controller is provided. Simulation results are also provided to demonstrate how the shared-controller works in the presence, or otherwise, of communication noise.

The paper is organized as follows. Section 2 describes the setup of the system, models human behaviour and finally formulates the wave damping problem for vehicles with shared-control, while the solution to the problem is given in Section 3, in which formal properties of the closed-loop system are presented. The robustness of the proposed shared-controller is discussed in Section 4. In addition, simulation results for four case studies are reported in Section 5. By comparing the performance of the vehicles with and without the shared-controller, we demonstrate the effectiveness of the established controller. Finally, conclusions and suggestions for future work are given in Section 6.

2. System modeling and problem formulation

This section describes the system dealt with in the paper and the car-following model used to represent the human behaviour. Moreover, the formulation of the shared-control problem for wave damping is provided.

2.1. System Description

The stop-and-go wave phenomenon in a circular road has been reproduced experimentally and studied in (Sugiyama et al., 2008; Stern et al., 2018; Fabritiis et al., 2008): it has been shown that the wave occurs naturally when the density of the vehicles on the road is higher than a certain value. For the sake of clarity, we consider the same setup as that in (Stern et al., 2018): a round track with single lane, the radius of which is R meters. However, such setup does not imply any loss of generality, since the analysis and the control scheme do not depend on the specific configuration. Unlike many other setups, all the vehicles on the round track are *equal*, *i.e.* there is no leading car in the fleet.

Consider a platoon of $M, M > 1$, homogeneous vehicles driven within the lane, denoted as Vehicle 1, Vehicle 2, …, Vehicle M. Note that the Vehicle $(i-1)$ is the one in front of Vehicle i, for all $i \in \{2,3,\ldots,M\}$, and Vehicle M is the preceding vehicle of Vehicle 1. The Vehicle M is also denoted as the Vehicle 0. Then, the preceding vehicle of Vehicle i is denoted as Vehicle $(i-1)$ for all $i \in \{1,2,\ldots,M\}$. The distance between adjacent vehicles can then be defined as follows.

Definition 1. The distance between Vehicle i and its preceding vehicle is defined as $d_{i-1,i}$ for all $i \in \{1,2,\ldots,M\}$. ◀

Assumption 1. All vehicles are unable to move backward and the maximum forward speed for Vehicle i, denoted as v^i_{max}, is known for all $i \in \{1, 2, \ldots, M\}$. In addition, the minimum acceleration for Vehicle i, denoted as a^i_{min}, is negative and constant, while the maximum acceleration for Vehicle i, denoted as a^i_{max}, is positive and constant. Both are given for all $i \in \{1,2,\ldots,M\}$. ◀

2.2. Car-Following Model

The car-following model which describes the influence on a car resulting from the presence of a preceding vehicle in the same lane has attracted an increasing amount of attention and gained importance in traffic research and in the study of intelligent transportation systems (Brackstone and McDonald, 1999; Gipps, 1981). In the rest of the paper, we assume that each vehicle follows its preceding vehicle according to the nonlinear law, based on the car-following model proposed in (Helly, 1959),

$$\begin{aligned} x_i(k+1) &= x_i(k) + T_s v_i(k), \\ v_i(k+1) &= v_i(k) + T_s a_{h_i}(k), \end{aligned} \tag{1}$$

where

$$a_{h_i}(k) = \min\left(\max\left[a_{i,cal}(k), a^i_{min}, -\frac{v_i(k)}{T_s} \right], m_i(k), a^i_{max}, \frac{v^i_{max} - v_i(k)}{T_s} \right) \tag{2}$$

with

$$a_{i,cal}(k) = C_{i,2}\left[x_{i-1}(k-n_d) - x_i(k-n_d) - D_i(k-n_d)\right] + C_{i,1}\left[v_{i-1}(k-n_d) - v_i(k-n_d)\right],$$

and

$$m_i(k) = \frac{x_{i-1}(k) - x_i(k)}{T_s^2} + \frac{v_{i-1}(k) - 2v_i(k)}{T_s} - \frac{d_{min}}{T_s^2}. \tag{3}$$

Note that $C_{i,1}$ and $C_{i,2}$ are two constant parameters, representing the behaviour of the human driver for Vehicle i in the setup described in Section 2.1. Usually, the values of both parameters vary from one human driver to another and from one situation to another (such as from urban areas to freeways and from sunny days to rainy days). $x_i(k)$ and $v_i(k)$ denote the location and the speed of Vehicle i in the platoon of M homogeneous vehicles at the time instant kT_s, respectively, while $a_{h_i}(k)$ denotes the acceleration generated by the human driver of Vehicle i at the time instant kT_s. Similarly, $x_{i-1}(k)$ and $v_{i-1}(k)$ represent the position and the velocity of the preceding vehicle, *i.e.* Vehicle $(i-1)$, at the time instant kT_s. In addition, $D_i(k-n_d)$, describing the desired distance[1] between Vehicle i and its preceding one at the time instant kT_s, is a function of $v_i(k-n_d)$, rather than a function of $v_i(k)$ due to the human driver's reaction delay. More specifically, it is calculated as

$$D_i(k-n_d) = d_{min} + \beta_i v_i(k-n_d), \tag{4}$$

where d_{min} is the minimum distance between two adjacent vehicles (set to avoid collisions) and β_i is a positive constant. Note that β_i may vary for different people, while the value of d_{min} depends on the size of the car. In fact, the smaller β_i is, the more aggressive (that is, tending to keep smaller distance to the preceding vehicle) the human driver is. Note that the value of d_{min} can vary among human drivers, *i.e.* larger values and smaller values can be set for meek and aggressive human drivers, respectively.

Remark 1. We have chosen the car-following model given by (1) not only because it satisfies all the mechanical and safety constraints (details are given in Property 1), but also because it is able to generate the same traffic wave observed in the experiments in

[1] In the car-following maneuvers, the human driver adjusts the acceleration of the vehicle generated by braking or gas pedal so that the distance between the car and the preceding one equals to the desired distance.

(Stern et al., 2018) (details are given in Figs. 1 and 2).

Fact 1. (*DVSA, 2016*) According to the rules of driving a car, the human driver should drive at least 2 s behind the vehicle in front during ideal conditions.

A typical instance of group of parameter values for a typical human driver is given in Table 1. Using these parameters, the stop-and-go wave is reproduced in simulation as discussed in Section 2.3. Note that d_{min} is related to the length of the vehicle and it is chosen to be 5 meters as most passenger vehicles are between 4 and 4.5 meters in length, while β is chosen to match the *2 s rule* given in Fact 1. The following assumptions are supposed to hold for the rest of the paper.

Assumption 2. $a_{h_i}(k) = 0$, for all $k \in \{0, 1, \ldots, n_d - 1\}$ and all $i \in \{1, 2, \ldots, M\}$. ◀

Assumption 2 indicates that the acceleration of Vehicle i is zero during the initial few samples if the vehicle is controlled solely by the human driver. This is due to human drivers' reaction delay. Hence, $v_i(0) = v_i(1) = \ldots = v_i(n_d - 1), x_i(k) = x_i(0) + kT_s v_i(0)$ and $d_{i-1,i}(k) = d_{i-1,i}(0) + kT_s(v_{i-1}(0) - v_i(0))$, for all $k \in \{0, 1, \ldots, n_d - 1\}$ and all $i \in \{1, 2, \ldots, M\}$.

Assumption 3. The initial position, $x_i(0)$, and velocity, $v_i(0)$, of Vehicle i are chosen such that all safety and mechanical constraints are satisfied for a certain period, *i.e.* $0 \leqslant v_i(0) \leqslant v^i_{max}$ and $d_{min} \leqslant d_{i-1,i}(k) + T_s v_i(0)$ for all $i \in \{1, 2, \ldots, M\}$ and $k \in \{0, 1, \ldots, n_d - 1\}$. ◀

Because all human drivers have reaction delays, Assumption 3 is used to guarantee that all the safety and mechanical constraints are satisfied before the human drivers are able to take any action. The formal properties of the system of which all vehicles are controlled completely by human drivers are given in Proposition 1, from which we conclude that the car-following model (1) is able to satisfy all the mechanical and safety constraints.

Proposition 1. Consider a vehicle set {Vehicle 1, Vehicle 2, …, Vehicle M} describing a platoon of M homogeneous vehicles. The relationship of adjacent vehicles is described by the car-following model given in (1), (2). Assume that Assumptions 1–3 hold. Then, the following mechanical constraints C1)-C2) and safety constraint C3) are satisfied:

C1) $v_i(k) \in [0, v^i_{max}]$, for all $i \in \{1, 2, \ldots, M\}$ and $k \in \{1, 2, \ldots\}$.
C2) $a_{h_i}(k) \in [a^i_{min}, a^i_{max}]$, for all $i \in \{1, 2, \ldots, M\}$ and $k \in \{1, 2, \ldots\}$.
C3) $x_{i-1}(k) - x_i(k+1) \geqslant d_{min}$, for all $i \in \{1, 2, \ldots, M\}$ and $k \in \{1, 2, \ldots\}$. □

Proof 1. The statements can be proved by mathematical induction.When $k = 0$, C1) to C3) hold by Assumption 3. We now assume that C1) to C3) hold for all $i \in \{1, 2, \ldots, M\}$ and $k = l$, then we prove that C1) to C3) hold for all $i \in \{1, 2, \ldots, M\}$ and $k = l + 1$.To begin with, it is obvious that C2) holds for $k = l + 1$ by the definition of $a_{h_i}(k)$ given in (2). Furthermore,

$$v_i(l+1) = v_i(l) + T_s a_{h_i}(l) \leqslant v_i(l) + T_s \frac{v^i_{max} - v_i(l)}{T_s} = v^i_{max},$$

$$v_i(l+1) = v_i(l) + T_s a_{h_i}(l) \geqslant v_i(l) + T_s \frac{-v_i(l)}{T_s} = 0.$$

Therefore, C1) holds for $k = l + 1$. In addition,

$$\begin{aligned} x_{i-1}(l+1) - x_i(l+2) &= x_{i-1}(l) + T_s v_{i-1}(l) - x_i(l+1) - T_s v_i(l+1) \\ &= x_{i-1}(l) + T_s v_{i-1}(l) - x_i(l) - T_s[2v_i(l) + T_s a_{h_i}(l)] \\ &= T_s[v_{i-1}(l) - 2v_i(l) - T_s a_{h_i}(l)] \\ &\quad + x_{i-1}(l) - x_i(l). \end{aligned}$$

According to the definition of a_{h_i} given in (2), it follows that

$$a_{h_i}(l) \leqslant \frac{x_{i-1}(l) - x_i(l)}{T_s^2} + \frac{v_{i-1}(l) - 2v_i(l)}{T_s} - \frac{d_{min}}{T_s^2},$$

hence

$$x_{i-1}(l+1) - x_i(l+2) \geqslant d_{min},$$

that is, C3) holds for $k = l + 1$.

Since both the base case and the inductive step have been carried out, the property holds for all $i \in \{1, 2, \ldots, M\}$ and $k \in \{1, 2, \ldots\}$. □

Remark 2. To guarantee the collision-free property, the distance $x_{i-1}(k) - x_i(k+1)$ is used, rather than $x_{i-1}(k+1) - x_i(k+1)$, because $x_{i-1}(k+1) - x_i(k+1) \geqslant x_{i-1}(k) - x_i(k+1)$. In addition, there is no communication between vehicles, which means $x_{i-1}(k+1)$ is unknown to Vehicle i and the human driver of Vehicle i takes actions based on the measurement of $d_{i-1,i}(k)$.

Remark 3. Properties C1) to C3) given in Proposition 1 do not depend on the value of $C_{i,1}$ and $C_{i,2}$. In other words, all the properties in Proposition 1 are valid for different human drivers.

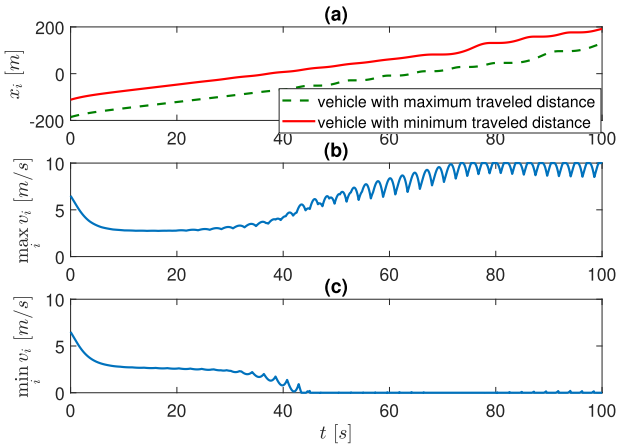

Fig. 1. (a): Time histories of the positions of Vehicles 16 (green dashed line) and Vehicle 10 (red solid line); (b) and (c): Time histories of $\max_i v_i$ and $\min_i v_i$, for all $i \in \{1, 2, \ldots, 21\}$, respectively.

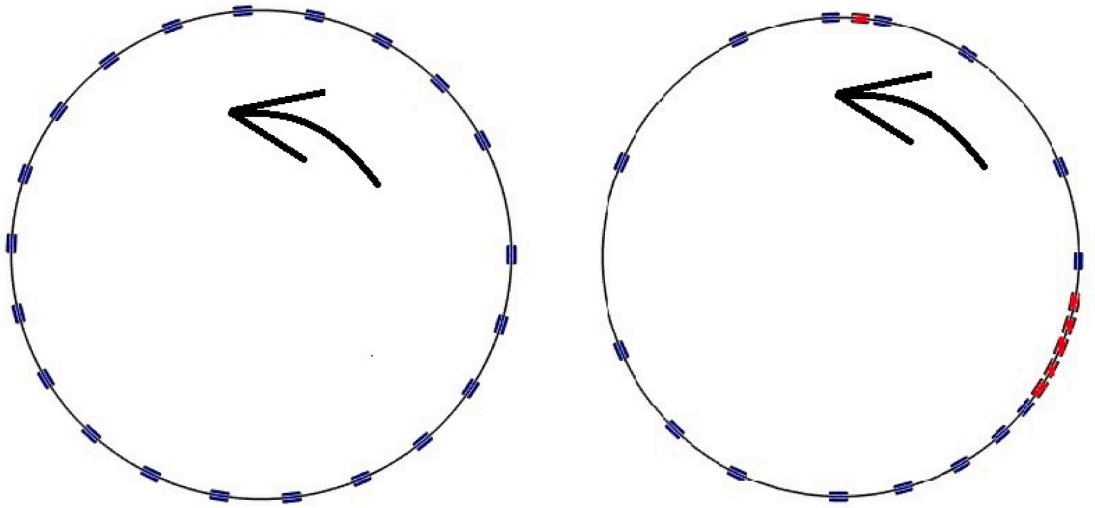

(a) Alignment of the vehicles at the beginning of the simulation.

(b) Alignment of the vehicles when the wave can be seen clearly. Blue rectangles: moving vehicles. Red rectangles: stopped vehicles.

Fig. 2. Snapshots at the track displaying the positions of 21 vehicles in the (x,y)-plane.The direction of the arrow indicates the driving direction.

Table 1
Parameters of the Car Following Model Representing a Typical Human Driver in the Setup (Brackstone and McDonald, 1999).

Parameter	Value	Parameter	Value
$C_{i,1}$	0.5	$C_{i,2}$	0.125
d_{min}	5	β_i	2
n_d	15	T_s	0.1

Given a fleet of M homogeneous vehicles evenly distributed on a single-lane circular track with radius R meters, suppose that each vehicle has a human driver, the performance of which is described by the Eqs. (1). The stop-and-go wave, similar to that presented in (Stern et al., 2018), can be observed in simulation performed with $M = 21$ and $R = 41.4$ m, the results of which are displayed in Figs. 1 and 2. At the beginning of the simulation the vehicles are evenly distributed along the track, as shown in Fig. 2(a), *i.e.* $d_{i-1,i} = 12.38$ m, for all $i \in \{1, 2, \ldots, 21\}$. The initial speed for all vehicles is set to 6.5 m/s. The wave can be observed clearly even though there is no merging, accidents and lane-changing maneuvers. Fig. 1-(a) displays the time histories of the position of Vehicles 16 (who has traveled

the longest distance within 100 s) and 10 (who has traveled the shortest distance within 100 s). The total traveled distances for Vehicles 16 and 10 are 312 m and 299 m, respectively. Clearly both vehicles stop for some periods as the curves are almost flat for those periods. Moreover, note that the time histories of the positions for all the other vehicles have similar shapes and properties: the curve representing the position of the vehicle includes several flat segments with similar lengths. Furthermore, we are able to observe that there are some phase shifts between two curves representing two adjacent vehicles representing the propagation of the wave. Fig. 1-(b) and (c) show that there are vehicles running at their maximum speed, *i.e.* 10 m/s, from 70 s and there are vehicles stopping, *i.e.* $v_i = 0$ m/s for some i, from 45 s, respectively, indicating that the stop-and-go traffic wave occurs at $t = 45$ s (Note that i in Fig. 1-(b) and (c) varies with time.) Finally, it is worth of saying that the maximum and the minimum speed of the fleet do increase and decrease smoothly to 10 m/s and 0 m/s, respectively, indicating that the wave generates and propagates step by step.

2.3. Problem statement

In what follows, the wave damping problem is solved via shared-control: a control scheme combining a feedback control input and the human driver's input. Before formulating the problem, definitions related to how the control authority is shared between the human driver and the feedback controller need to be introduced.

Definition 2. The shared-control input a_{s_i} for Vehicle i, denoted as *s-control*, is a combination of the feedback control input a_{c_i}, denoted as *c-control*, and the human driver's input a_{h_i}, denoted as *h-control*. It is defined as

$$a_{s_i} = (1 - f_i)a_{c_i} + f_i a_{h_i}, \tag{5}$$

where f_i, defined as *sharing function*, quantifies how the control authority is shared between the driver and the feedback controller. ◀ Note that $f_i \in [0,1]$. In addition, $f_i = 1$ and $f_i = 0$ refer to the cases in which Vehicle i is controlled completely by the human driver and by the feedback controller, respectively.

Definition 3. The instantaneous satisfaction index[2] $\mathscr{S}_i(k)$ for the human driver of Vehicle i at the time instant kT_s is defined as:

$$\mathscr{S}_i(k) = \begin{cases} 0, & \text{if Vehicle } i \text{ is forced to follow a speed less than } v_{i-1}(k - n_d), \\ 1, & \text{if Vehicle } i \text{ is able to follow a speed no less than } v_{i-1}(k - n_d), \end{cases} \tag{6}$$

where n_d represents the human driver's reaction delay. ◀ Note that $\mathscr{S}_i(k) = 0$ ($\mathscr{S}_i(k) = 1$) indicates that the human driver of Vehicle i is disappointed (satisfied) with the situation at the time-instant kT_s. In addition, $\mathscr{S}_i(k) = 1$ even if $v_i(k) < v_{i-1}(k - n_d)$ as long as the target speed of Vehicle i is not less than $v_{i-1}(k - n_d)$ at the time instant kT_s.

Assumption 4. The vehicles are "Level 2" vehicles, that is vehicles for which the human driver is responsible for their behaviour and has to focus consistently on the driving, despite the fact that the vehicle has a certain level of autonomy.

According to the above assumption, it is assumed that even when the control authority is taken completely by the feedback controller, the human driver attention does not drop and he/she behaves consistently, ready to be handed back control authority at anytime.

According to Definition 2, the dynamics of Vehicle i controlled by the s-control can be described by the equations

$$\begin{aligned} x_i(k+1) &= x_i(k) + T_s v_i(k), \\ v_i(k+1) &= v_i(k) + T_s a_s(k), \end{aligned} \tag{7}$$

with the h-control defined in (2). Assume that each vehicle is able to receive driving instructions, such as a recommended speed v^r from the higher-level traffic control center, but the human drivers ignore these instructions because they believe that their own average speed increases if they follow the preceding vehicle closely. Note that, in nominal situations (*i.e.* without disturbances or faults), each vehicle receives the same instructions, while if the equipment on one of the vehicles does not work properly, it may receive different instructions. The shared-control problem for traffic wave damping with the setup described in Section 2.1 can then be formulated as follows.**Formulation of the Shared Control Problem**

Consider a fleet of M homogeneous vehicles on a single-lane circular track with radius R meters, the dynamics of which is described by (5)–(7). Assume that the human drivers' behaviour is modeled as in (1) and (2) and Assumptions 1–3 hold. The control objective is to find (if possible).

- a c-control
- a sharing function

for each vehicle such that the closed-loop system (2), (5), (7) has the following properties.

[2] The instantaneous satisfaction index describes how satisfied the human driver is under the action of the proposed shared control scheme at each time instant.

P1) The stop-and-go wave is damped, *i.e.* there exists a signal $v^i_{min}(k)$ for Vehicle i, the value of which is always positive, such that $v_i(k) \in [v^i_{min}(k), v^i_{max}]$, for all $i \in \{1,2,\ldots,M\}$ and $k \in \{1,2,\ldots\}$.

P2) The saturation constraints on the acceleration of all vehicles are always satisfied, *i.e.* $a_{s_i}(k) \in [a^i_{min}, a^i_{max}]$, for all $i \in \{1,2,\ldots,M\}$ and $k \in \{1,2,\ldots\}$.

P3) $x_{i-1}(k) - x_i(k+1) \geqslant d_{min}$, for all $i \in \{1,2,\ldots,M\}$ and $k \in \{1,2,\ldots\}$.

P4) $\mathscr{S}_i(k) = 1$, for all $i \in \{1,2,\ldots,M\}$ and $k \in \{1,2,\ldots\}$.

Note that the reason for using $x_{i-1}(k)$, rather than $x_{i-1}(k+1)$, in P3) has been clarified in Remark 2.

3. Shared-control design for the traffic wave damping problem

This section provides a solution to the shared-control problem formulated in Section 2.3. The design includes two steps: the construction of a feedback controller for each vehicle (Section 3.1) and and the definition of the sharing law to define how the control authority is shared between the feedback controller and the human driver (Section 3.2). The stability analysis of the closed-loop system is then given in Section 3.3.

The block diagram of the overall system is shown in Fig. 3, from which we see that the "Shared Control" contains two blocks: the "c-control" and the "Sharing Law". In addition, the shared-controller makes use of information on the local environment (including the speed of the vehicle, the distance and the relative speed between the vehicle and the preceding one), the human driver's input and the recommended speed v^r from a higher level traffic control center. Note that v^r can be a time-varying signal.

3.1. Design of the c-control

Inspired by the VSL control (Hegyi et al., 2008), we choose a feedback controller similar to the car-following controller. The dynamics of Vehicle i controlled solely by the feedback controller a_{c_i} can then be described by the equations

$$\begin{aligned} x_i(k+1) &= x_i(k) + T_s v_i(k), \\ v_i(k+1) &= v_i(k) + T_s a_{c_i}(k), \end{aligned} \tag{8}$$

where

$$a_{c_i}(k) = \min\left(\max\left(a_{cc_i}(k), a^i_{min}, -\frac{v_i(k)}{T_s} \right), m_i(k), a^i_{max}, \frac{v^i_{max} - v_i(k)}{T_s} \right), \tag{9}$$

with

$$a_{cc_i}(k) = C_{c2}[x_{i-1}(k-n_c) - x_i(k-n_c) - D_{c_i}(k-n_c)] + C_{c1}[v^r(k-n_c) - v_i(k-n_c)],$$

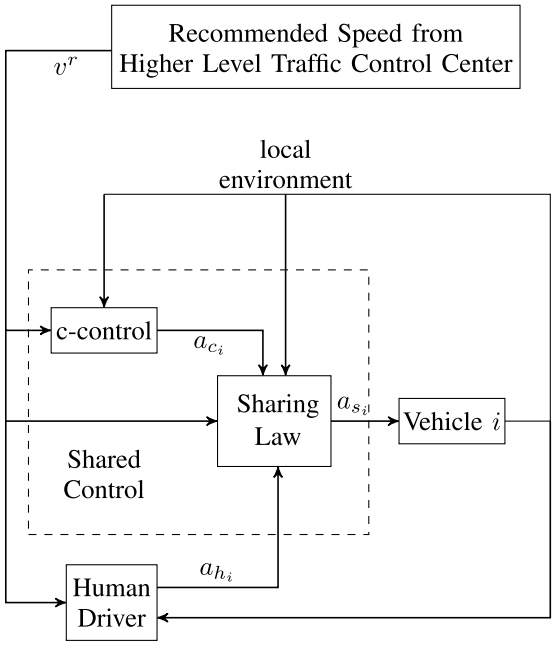

Fig. 3. Block diagram of the shared control architecture referred to Vehicle i. Dashed box: the shared control block.

and $m_i(k)$ is given in (3). Note that $D_{c_i}(k-n_c)$, that is the desired distance between adjacent vehicles, is usually related to v^r. According to the *2 s rule* given in Fact 1, $D_{c_i}(k-n_c)$ may be calculated as

$$D_{c_i}(k-n_c) = d_{min} + 2v^r(k-n_c). \tag{10}$$

However, in this study, $D_{c_i}(k-n_c)$ is assumed to be a constant, *i.e.*

$$D_{c_i}\left(k-n_c\right) = \frac{\text{theperimeterofthecircartrack}}{\text{thenumberofvehicles}}.$$

The following assumption is introduced to guarantee that the speed saturation constraints (P1 in Section 2.3) and and the safety constraints (P3 in Section 2.3) are satisfied before the feedback controller is able to take any action.

Assumption 5. The variable a_{c_i} is such that $a_{c_i}(k) = 0$ for all $k \in \{0, 1, 2, \ldots, n_c - 1\}$ and all $i \in \{1, 2, \ldots, M\}$. In addition, for any given n_c, C_{c1} and C_{c2}, the initial location and speed of Vehicle i are chosen such that the constraints

- $v_{cm} + a_{min}T_s(n_c+1) \leqslant v_i(0) \leqslant v^i_{max}$, for all $i \in \{1, 2, \ldots, M\}$, where
$$v_{cm} = \frac{C_{c1}v^r(k-n_c) + C_{c2}(d_{min} - D_{c_i}(k-n_c))}{C_{c1} - C_{c2}T_s}, \tag{11}$$
- $d_{min} \leqslant x_{i-1}(0) - x_i(0) + kT_s[v_{i-1}(0) - v_i(0)] - T_s v_i(0)$, for all $i \in \{1, 2, \ldots, M\}$ and $k \in \{0, 1, 2, \ldots, n_c - 1\}$,

hold. ◀

Assumption 6. For any given $d_{min}, a_{min}, T_s, n_c$ and a given signal v^r, the parameters C_{c1} and C_{c2} of the controller (9) are chosen such that $v_{cm} + a_{min}T_s(n_c+1) > 0$. ◀

Assumption 6 is used to guarantee that the minimum speed of Vehicle i is a positive value in the situation discussed in the following lemma, *i.e.* Vehicle i *never stops*.

Lemma 1. Consider the closed-loop system (8) controlled by the feedback controller (9). Suppose that Assumptions 5 and 6 hold. Then, the closed-loop system has the following properties:

- $v_i(k) \in [v_{cm} + a_{min}T_s(n_c+1), v^i_{max}]$, for all $i \in \{1, 2, \ldots, M\}$ and $k \in \{1, 2, \ldots\}$, where v_{cm} is defined in (11);
- $a_{c_i}(k) \in [a^i_{min}, a^i_{max}]$, for all $i \in \{1, 2, \ldots, M\}$ and $k \in \{1, 2, \ldots\}$;
- $x_{i-1}(k) - x_i(k+1) \geqslant d_{min}$, for all $i \in \{1, 2, \ldots, M\}$ and $k \in \{1, 2, \ldots\}$. □

Proof 2. The first statement can be proved by mathematical induction.

The claim holds for all $i \in \{1, 2, \ldots, M\}$ and $k \in \{0, 1, \ldots, n_c - 1\}$. Suppose now that the first claim holds for all $i \in \{1, 2, \ldots, M\}$ and $k \in \{0, 1, \ldots, l\}$, where $l \geqslant n_c - 1$. We now prove that the claim holds for all $i \in \{1, 2, \ldots, M\}$ and $k = l + 1$. This can be shown by contradiction.

Assume that there exists $i \in \{1, 2, \ldots, M\}$ such that

$$\begin{aligned} v_i(l+1) &< v_{cm} + a_{min}T_s(n_c+1), \\ v_i(l) &\geqslant v_{cm} + a_{min}T_s(n_c+1). \end{aligned} \tag{12}$$

The former inequality yields $v_i(l-n_c) < v_{cm}$. In addition, a_{cc_i} can be calculated as

$$\begin{aligned} a_{cc_i}(l) &= C_{c2}[x_{i-1}(l-n_c) - x_i(l-T_c) - D_{c_i}(l-n_c)] + C_{c1}[v^r(l-n_c) - v_i(l-n_c)] \\ &\geqslant C_{c2}[v_i(l-n_c)T_s + d_{min} - D_{c_i}(l-n_c)] + C_{c1}[v^r(l-n_c) - v_i(l-n_c)] \\ &= C_{c1}v^r(l-n_c) + C_{c2}(d_{min} - D_{c_i}(l-n_c)) - (C_{c1} - C_{c2}T_s)v_i(l-n_c) \\ &= -(C_{c1} - C_{c2}T_s)[v_i(l-n_c) - v_{cm}] > 0. \end{aligned}$$

Hence, $a_{cc_i}(l) > 0$, yielding $v_i(l+1) > v_i(l)$, which is contradictory to (12). Therefore, $v_i(l+1) \geqslant v_{cm} + a_{min}T_s(n_c+1)$, with v_{cm} given in (11). Furthermore, the inequality $v_i(l+1) \leqslant v^i_{max}$ is a direct consequence of the fact that $a_{c_i}(l) \leqslant \frac{v^i_{max} - v_i(k)}{T_s}$ by the definition of a_{c_i} given in (9). To sum up, the first claim holds.

The second statement is a trivial consequence of the definition of a_{c_i} given in (9) and the third statement can be proved similarly to the claim given in Proposition 1. □

Remark 4. Lemma 1 states that Properties P1) to P3) in Section 2.3 hold if all the vehicles are controlled solely by the feedback controller (9).

For typical applications, the communication delay is much smaller compared to the human driver's reaction time, *i.e.* $n_c \ll n_d$. In

other words, the delay of the feedback controller is much smaller than the human reaction delay. Table 2 indicates a group of parameter values in the design of the c-control. According to Assumption 6, it is obvious that the selection of C_{c1} and C_{c2} implies $v_{cm} + a_{min}T_s(n_c + 1) > 0$, for all $v^r > 3$. In addition, the range of parameter values for the vehicles are displayed in Table 3.

Remark 5. Using the method detailed in the proof of Lemma 1, one could show that for the more general cases in which $D_{c_i}(l - n_c)$ is calculated using (10), the properties expressed by Lemma 1 hold as well. In addition, v_{cm} can be calculated as

$$v_{cm} = \frac{(C_{c1} - 2C_{c2})v^r(k - n_c)}{C_{c1} - C_{c2}T_s}.$$

3.2. Shared-Control Law

This subsection provides the design of the shared-control law which aims to combine the human input together with the feedback control input without disappointing the human driver. Note that the index indicating if the human driver is instantaneously satisfied, or otherwise, is given in Definition 3.

The sharing function of Vehicle i at the time instant kT_s (that is $f_i(k)$), is defined as

$$f_i\left(k\right) = \begin{cases} 1, & \sigma_1 \leqslant v_{i-1}(k - n_d) - v^r(k - n_c), \\ l_i(k), & \sigma_2 < v_{i-1}(k - n_d) - v^r(k - n_c) < \sigma_1, \\ 0, & v_{i-1}(k - n_d) - v^r(k - n_c) \leqslant \sigma_2, \end{cases} \tag{13}$$

where $l_i(0) = 1$ and

$$l_i(k) = \begin{cases} 1, & \text{if } f_i(k-1) = 1, \\ 0, & \text{if } f_i(k-1) = 0, \end{cases}$$

for all $k \in \{1, 2, \ldots\}$. In addition, σ_1 and σ_2 are two user-selected constants such that $\sigma_2 < \sigma_1$.

Fig. 4 provides a graphical illustration of the sharing function $f_i(k)$ defined in (13). The sharing function is a hysteresis switch, which is used to reduce oscillations (Jiang et al., 2016). In order to make the satisfaction index defined in (6) equals to 1, we choose $\sigma_1 = 0$ and σ_2 a negative constant, selected by the human driver. Note that, the smaller the value of σ_2, the less aggressive the human driver is, because this allows the feedback controller to work for a broader range of situations. If σ_2 is a large negative constant, the human driver tends to allow the feedback controller to gain control authority on the vehicle when the recommended speed $v^r(k - n_c)$ is slightly above the estimated speed $v_{i-1}(k - n_d)$ of the preceding vehicle. In addition, Fig. 4 shows that we can increase the period in which the control authority is held by the human driver by reducing the value of σ_2.

Finally, the overall shared-control law for Vehicle i at the time instant kT_s, that is $a_{s_i}(k)$, is given by (5), where $f_i(k), a_{c_i}(k)$ and $a_{h_i}(k)$ are calculated using (13), (9) and (2), respectively.

3.3. Stability Analysis

This subsection studies properties of the closed-loop system described by (2), (5), (7), (9) and (13).

Theorem 1. Consider the system (2), (7) controlled by (5), (9) and (13). Suppose Assumptions 1–6 hold and the recommended speed $v^r(k)$ is such that[3] $v_{cm} + a^i_{min}T_s(\max(n_c, n_d) + 1) + C_{c1}\sigma/(C_{c1} - C_{c2}T_s) > 0$, for all $k \in \{1, 2, \ldots\}$ and all $i \in \{1, 2, \ldots, M\}$. Let a_{h_i}, for all $i \in \{1, 2, \ldots, M\}$, be an unknown h-control[4] such that Proposition 1 holds. Then, for any negative user-selected σ_2 and for $\sigma_1 = 0$, the closed-loop system has the following properties.

- P1) No vehicle stops, *i.e.* there exists a strictly positive signal $v_{min}(k)$ such that $v_i(k) \in [v_{min}(k), v_{max}]$, for all $i \in \{1, 2, \ldots, M\}$ and $k \in \{1, 2, \ldots\}$.
- P2) The mechanical constraints on the vehicles' acceleration are always satisfied, *i.e.* $a_{s_i}(k) \in [a^i_{min}, a^i_{max}]$, for all $i \in \{1, 2, \ldots, M\}$ and $k \in \{1, 2, \ldots\}$.
- P3) There is no collision, *i.e.* $x_{i-1}(k) - x_i(k + 1) \geqslant d_{min}$, for all $i \in \{1, 2, \ldots, M\}$ and $k \in \{1, 2, \ldots\}$.
- P4) The human driver is satisfied at each time instant during the journey, *i.e.* $\mathscr{S}_i(k) = 1$, for all $i \in \{1, 2, \ldots, M\}$ and $k \in \{1, 2, \ldots\}$. □

Proof 3. To begin with, P2) is a direct consequence of the definition of $a_{s_i}(k)$ given in (5) and of the fact that $a_{h_i} \in [a^i_{min}, a^i_{max}]$ and $a_{c_i} \in$

[3] Note that the constraints on $v^r(k)$ is to guarantee that the recommended speed is reasonably high. Such constraint is essential to prove P1) as detailed in the proof of Theorem 1.

[4] We assume that the parameter values of the car-following model, *i.e.* $C_{i,1}$ and $C_{i,2}$, are unknown constants within certain ranges, *i.e.* $C_{i,1} \in \left[\underline{C}_1, \overline{C}_1\right]$ and $C_{i,2} \in \left[\underline{C}_2, \overline{C}_2\right]$.

Table 2
Parameters of the Feedback Controller.

Parameter	Value	Parameter	Value	Parameter	Value
C_{c1}	10	C_{c2}	1	n_c	2

Table 3
Parameters of the Vehicles (Stern et al., 2018; Bartlett, 2018; Greibe, 2007).

Parameter	Value Range	Parameter	Value Range
a_{max}	[2,2.5]	a_{min}	[-4,-3]
v_{max}	[30,35]	d_{min}	5

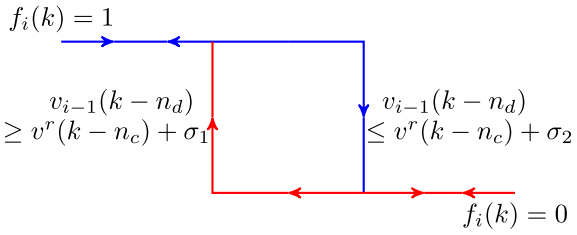

Fig. 4. Graphical Illustration of the Sharing Function $f_i(k)$.

$[a^i_{min}, a^i_{max}]$, by the definitions of a_{h_i} and a_{c_i} given in (2) and (9), respectively.

Based on the definitions of $a_{h_i}, a_{s_i}, a_{c_i}$ and $f_i(k)$ given in (2), (5), (9) and (13), respectively, it is easy to conclude that

$$\begin{aligned} a_{s_i} \leqslant & \quad \min\left(m_i\left(k\right), a^i_{max}, \frac{v^i_{max} - v_i(k)}{T_s}\right), \\ a_{s_i} \geqslant & \quad \max\left(a^i_{min}, -\frac{v_i(k)}{T_s}\right), \end{aligned} \tag{14}$$

where $m_i(k)$ is given by (3). P3) can then be proved by mathematical induction. Suppose P3) holds for all $i \in \{1, 2, \ldots, M\}$ and $k \in \{0, 1, \ldots, l\}$, then

$$\begin{aligned} & x_{i-1}(l+1) - x_i(l+2) \\ = \; & x_{i-1}(l) - x_i(l) + T_s[v_{i-1}(l) - 2v_i(l) - T_s a_{s_i}(l)] \geqslant d_{min}. \end{aligned}$$

Hence, P3) holds for all $i \in \{1, 2, \ldots, M\}$ and $k \in \{1, 2, \ldots\}$.

Based on the definition of a_{h_i}, a_{s_i} and a_{c_i} given in (2), (5) and (9), respectively, Vehicle i follows the speed $v_{i-1}(k - n_d)$ of the preceding car or the recommended speed $v^r(k - n_c)$ at the time instant kT_s, if $f_i(k) = 1$ or $f_i(k) = 0$, respectively. Moreover, the definition of $f_i(k)$ given in (13) yields that Vehicle i at the time instant kT_s aims to follow either $v_{i-1}(k - n_d)$ or $v^r(k - n_c)$. In addition, $f_i(k) = 1$ if $v_{i-1}(k - n_d) \geqslant v^r(k - n_c)$, hence $\mathscr{S}_i(k) = 1$, for all $k \in \{1, 2, \ldots, \}$. Therefore, P4) holds.

Finally, P1) can be proved similarly to what has been done in the proof of Lemma 1. Lemma 1 states that

$$v_i(k) \geqslant v_{cm} + a^i_{min} T_s(n_c + 1),$$

if $f_i(k) = 0$. Similarly,

$$\begin{aligned} v_i\left(k\right) \geqslant & \; \frac{C_{i,1} - \beta C_{i,2}}{C_{i,1} - T_s C_{i,2}} v_{i-1}\left(k - n_d\right) + a^i_{min} T_s\left(n_d + 1\right) \\ \geqslant & \; \frac{\underline{C}_1 - \beta \overline{C}_2}{\beta \overline{C}_1 - T_s \underline{C}_2} v_{i-1}\left(k - n_d\right) + a^i_{min} T_s\left(n_d + 1\right), \end{aligned}$$

if $f_i(k) = 1$. Then the minimum value of $v_i(k)$, that is $v_{min}(k)$, can be calculated, based on the definition of $f_i(k)$ and $a_{s_i}(k)$ given in (13) and (5), respectively, as

$$v_{min}(k) = \min\left\{ \frac{C_{c1}[v^r(k-n_c)+\sigma_2] + C_{c2}(d_{min} - D_{c_i}(k-n_c))}{C_{c1} - C_{c2}T_s}, \frac{\underline{C}_1 - \beta\overline{C}_2}{\beta\overline{C}_1 - T_s\underline{C}_2}\mathscr{V} \right\} + a^i_{min}T_s(\max(n_d,n_c)+1) > 0,$$

where $\mathscr{V} = \max(v^r(k-n_c), v_{i-1}(k-n_d))$, hence P1) holds.

Remark 6. In the analysis of Theorem 1 the recommended speed v^r can be a time-varying signal. This is important if one wants to extend the results to a broader range of situations. For example, in urban areas the recommended speed v^r would be different during peak hours and off-peak hours.

Remark 7. From the previous analysis we know that the design of the shared-controller does not depend on the parameter values in the car-following model (1). This is an important property in the implementation of the shared-controller, since it is difficult to measure the values of these parameters and, as previously explained, such values vary from one human driver to another and from one driving situation to another.

Remark 8. The closed-loop system with shared control does not suffer from severe instability (Seiler et al., 2004) since P1) in Theorem 1 holds: the speed of all vehicles never drops down to zero.

Remark 9. Even though we assumed that the maximum and the minimum speeds for Vehicle i, a^i_{min} and a^i_{max}, are constants, Theorem 1 still holds if these are time-varying variables as long as we change the control design and replace a^i_{max} and a^i_{min} with $a^i_{max}(k)$ and $a^i_{min}(k)$, respectively. This is because the proof of Theorem 1 does not depend on the choice of a^i_{min} and a^i_{max}. Note that in such a case the assumption in Theorem 1 "$v_{cm} + a^i_{min}T_s(\max(n_c,n_d)+1) + C_{c1}\sigma/(C_{c1} - C_{c2}T_s) > 0$" should be modified to "$v_{cm} + \underline{a}^i_{min}T_s(\max(n_c,n_d) + 1) + C_{c1}\sigma/(C_{c1} - C_{c2}T_s) > 0$", where $\underline{a}^i_{min} = \min_{k=1,2,\ldots} a^i_{min}(k)$.

4. Robustness analysis of the proposed shared-controller subject to disturbances

This section studies the performance of the proposed shared-control law in the presence of disturbances via a robustness analysis.

From Fig. 3 it is obvious that both the human driver and the shared-controller are able to receive information from the higher level traffic control center. In fact, such information is firstly broadcast by the traffic control center and received by the vehicle. Then, the vehicle is able to display it for the human driver to read. In the presence of disturbances, we assume that such information (*i.e.* the recommended speed v^r) is changed to $\widetilde{v}^r = v^r + \delta$, where δ denotes the difference between the received data $\widetilde{v}^r$ and the correct information v^r.

Corollary 1. Consider the system (2)–(7) controlled by (5)–(13). Suppose Assumptions 1–5 hold and the information received by Vehicle i is *corrupted*, *i.e.* the recommended speed received by Vehicle i is changed from $v^r(k-n_c)$ to $\widetilde{v}^r(k-n_c) = v^r(k-n_c) + \delta_i(k-n_c)$. Let a_{h_i}, for all $i \in \{1,2,\ldots,M\}$, be an unknown h-control such that Proposition 1 holds. Then for any negative user-selected σ_2 and $\sigma_1 = 0$ the properties P2) to P4) stated in Theorem 1 holds. □

Proof 4. Note that the proof of P2) to P4) in Theorem 1 does not depend on the value of v^r. Therefore, P2) to P4) hold even if the value of v^r has been modified by an attack.

Remark 10. Corollary 1 indicates that there is no collision even if the vehicle receives a corrupted recommended speed. In addition, even though the disturbance could affect the efficiency of the system, *i.e.* the average speed of the vehicles may be reduced, the stop-and-go wave can still be dampened if the disturbance δ does not have a sufficiently large negative value.

For example, based on the proof of Theorem 1, the parameter values given in Tables 1–3 and selecting $C_{i,1} \in \left[\underline{C}_1, \overline{C}_1\right]$, $C_{i,2} \in \left[\underline{C}_2, \overline{C}_2\right]$ for all $i \in \{1,2,\ldots,M\}$, are such that the stop-and-go wave does not occur if $\delta_i(k-n_c)$ is such that

$$\frac{\underline{C}_1 - \beta\overline{C}_2}{\beta\overline{C}_1 - T_s\underline{C}_2}[v^r(k-n_c) + \delta_i(k-n_c)] > -a^i_{min}T_s(n_d+1),$$

$$\frac{C_{c1}[v^r(k-n_c)+\sigma_2] + C_{c2}(d_{min} - D_{c_i}(k-n_c))}{C_{c1} - C_{c2}T_s} > -a^i_{min}T_s(n_c+1),$$

thus yielding $\delta_i(k-n_c) > -v^r(k-n_c) + 3$. Note that, any positive values of δ_i does not cause the stop-and-go wave, but may cause acceleration-deceleration waves.

Remark 11. The paper (Yuan et al., 2015) shows that the discharge rate is almost linearly related to speed. Consistently, an increase of the overall speed indicates an increase of the discharge rate.

5. Simulation results

This section discusses six case studies with parameter values of the feedback controllers and vehicles given in Tables 2 and 3, respectively: vehicles evenly distributed along a circular track with nonzero initial speed, vehicles line-up aligned along a circular track with zero initial speed, braking effects analysis, straight freeways simulation, performance of the vehicles with shared control when they approach areas where v^r changes suddenly and an attack/ defense test. Note that in most of the simulations, we have chosen $R = 150.4$ and $M = 21$. Simulation results are displayed in Sections 5.2, 5.3, 5.4, 5.5, 5.6 and 5.7. To begin with, the equilibrium condition for the simulation setup is calculated in Section 5.1.

5.1. Equilibrium Calculation

Suppose the location, the speed and the acceleration of Vehicle i at the equilibrium are defined as x_i^*, v_i^* and a_i^*, respectively. Then, according to the definition of equilibrium, one has

$$d_{i-1,i}^* = d_{min} + \beta v_i^*, \quad v_{i-1}^* = v_i^*, \quad a_i^* = 0,$$

for all $i \in \{1, 2, \ldots, 21\}$. Note that

$$\sum_{i=1}^{21} d_{i-1,i} = 2\pi \times 150.4,$$

hence

$$d_{i-1,i}^* = 45\ m, \quad v_i^* = 20\ m/s. \tag{15}$$

Remark 12. In other scenarios, such as in a freeway scenario, there is no need to calculate the equilibrium setup, because the design of the shared controller does not depend on the equilibrium state. Instead, it depends on the recommended speed v^r sent by the higher level traffic control center. In this section we use the equilibrium speed as the recommended speed v^r for most simulations. In this section, we also show that, even if $v^r \neq v_i^*$, the performance of the controlled system is improved by the use of the shared controller.

5.2. Evenly Aligned Vehicles Along the Track with Nonzero Initial Speed

In this subsection, we implement the shared-controller (5) in a scenario similar to that given in Section 2.3: the 21 vehicles are

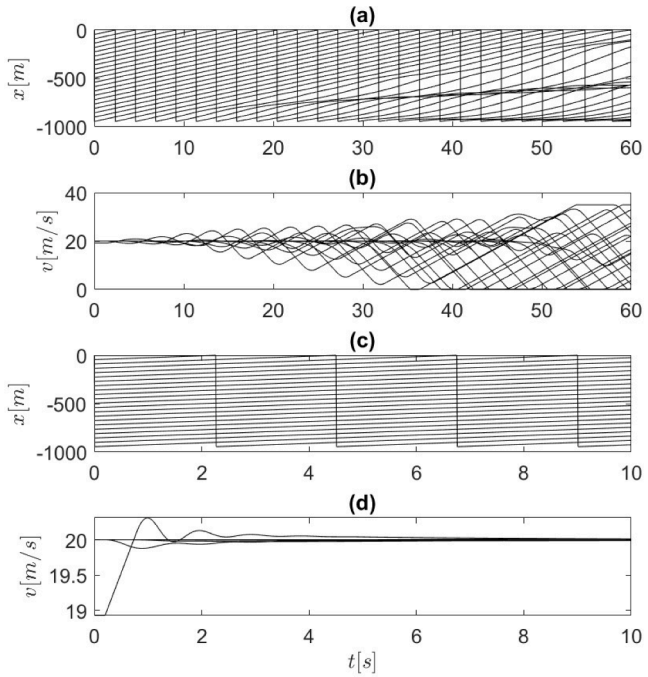

Fig. 5. Performance (*i.e.* wrapped position on the circular track, with respect to the length of the track, and speed) of all vehicles without (sub-figures (a) and (b)) and with shared control (sub-figures (c) and (d)). v^r is set to 20 m/s.

evenly distributed (*i.e.* $d_{i-1,i} = 45\ m$ for all $i \in \{1,2,\ldots,21\}$) along the track with the same initial speed 20 m/s corrupted by zero-mean normal distributed random noises with covariance 1. In the simulation we have chosen $\sigma_2 = -1\ m/s$. Simulation results are displayed in Figs. 5–9.

Fig. 5 shows that, although the initial states of all vehicles are close to the equilibrium, such small deviation from the equilibrium are amplified over time and finally traffic waves are generated. A certain number of vehicles have to stop and re-start the journey as illustrated in sub-figure (b). Such a stop-and-go wave is eliminated with the help of the proposed shared controller since there is no flat behaviour in sub-figure (c) and the speed of all vehicles converge to the recommended speed 20 m/s within 10 s, as shown in sub-figure (d). By comparing the sub-figures (a) and (c), we can conclude that the average travelled distance, within 1 min, for each vehicle increases from 950 m to 1200 m with the use of the shared controller, indicating that the proposed controller is able to improve traffic efficiency. In addition, by comparing Fig. 5c) and Fig. 7(c) we see that the average travelled distance and the average speed of Vehicle i within a given time period increases as v^r increases. Finally, by comparing Figs. 5 and 7, we can conclude that the traveled distance within a fixed period increases for both recommended speed equals to 20 m/s and 30 m/s. Such a phenomenon demonstrate that the recommended speed does not need to be very precise, hence the cost to get the recommended speed is not high.

Figs. 6 and 8 show the acceleration and jerk information for all vehicles during the simulation. It is clear that both acceleration and jerk for all vehicles become smoother with the use of the shared control in both cases, indicating that the comfort of the human driver is improved by the shared controller and it is independent of the recommended speed.

Fig. 9 shows how the traffic wave dampen performance varies with the number of vehicles exploiting the shared controller. Note that the vehicles controlled by the shared controller have been randomly selected from the vehicle set {Vehicle 1, Vehicle 2, …, Vehicle 21} and Fig. 9 only shows the performance of one vehicle. However, there is no loss of generality as Figs. 5 and 7 show that the performance of all vehicles are comparable. Therefore, such simulation reveals that the traffic wave damping problem can be solved even if only part of the vehicles are controlled by the shared controller. From Fig. 9 we are able to conclude that the wave is eliminated even if there is only six vehicles controlled by the shared controller, while all the other vehicles are controlled completely by human drivers. In addition, the more vehicles are controlled by the shared controller, the larger the average speed is and the smoother the time histories of the speeds for all vehicles.

To study the influence of the tunable parameter σ_2 (in the definition of the sharing law f_i) on the performance of the vehicle, we show simulation results for a randomly selected vehicle from the vehicle set {Vehicle 1, Vehicle 2, …, Vehicle 21} in Fig. 10. From this we see that the duration of the period in which the control authority is held by the human driver increases with the decrease of σ_2. In addition, the performance degrades (*i.e.* the speed variation increases) as σ_2 decreases.

5.3. Line-up Aligned Vehicles With Zero Initial Speed

In this section we study the case in which 21 vehicles are distributed in a queue along a single-lane circular track with radius of 150.4 m. The initial distances between adjacent vehicles are defined as

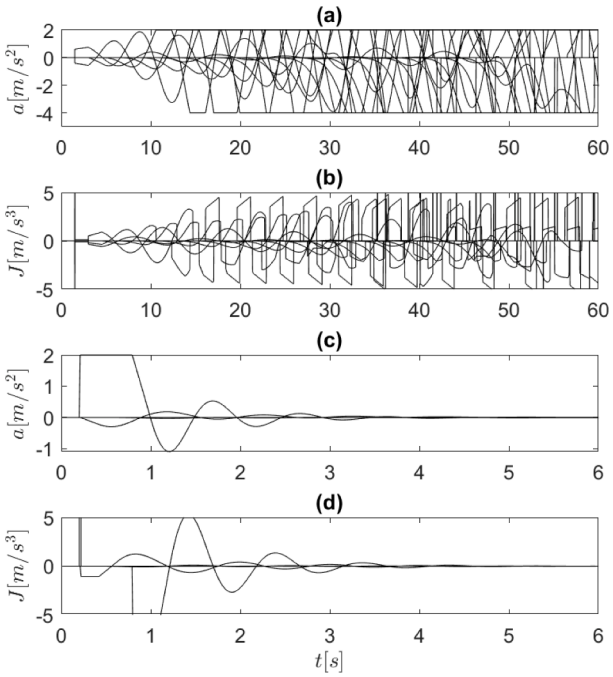

Fig. 6. Performance (*i.e.* acceleration and jerk) of all vehicles without (sub-figures (a) and (b)) and with shared control (sub-figures (c) and (d)). v^r is set to 20 m/s. The vehicle acceleration and jerk in the initial 6 s have been shown in sub-figures (c) and (d).

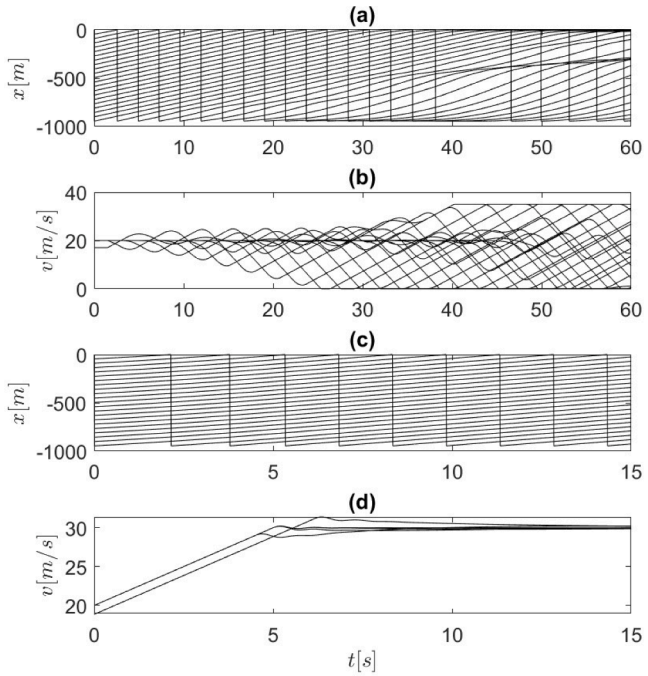

Fig. 7. Performance (*i.e.* wrapped position on the circular track, with respect to the length of the track, and speed) of all vehicles without (sub-figures (a) and (b)) and with shared control (sub-figures (c) and (d)). v^r is set to 30 m/s.

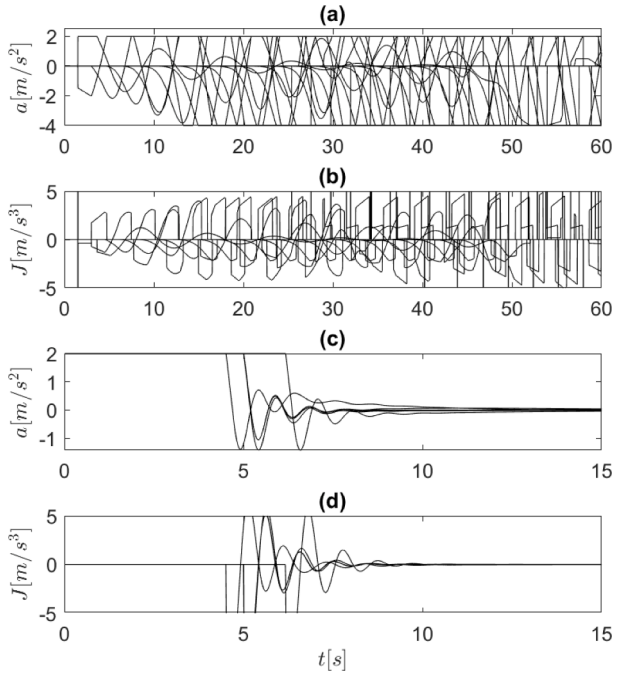

Fig. 8. Performance (*i.e.* acceleration and jerk) of all vehicles without (sub-figures (a) and (b)) and with shared control (sub-figures (c) and (d)). v^r is set to 30 m/s.

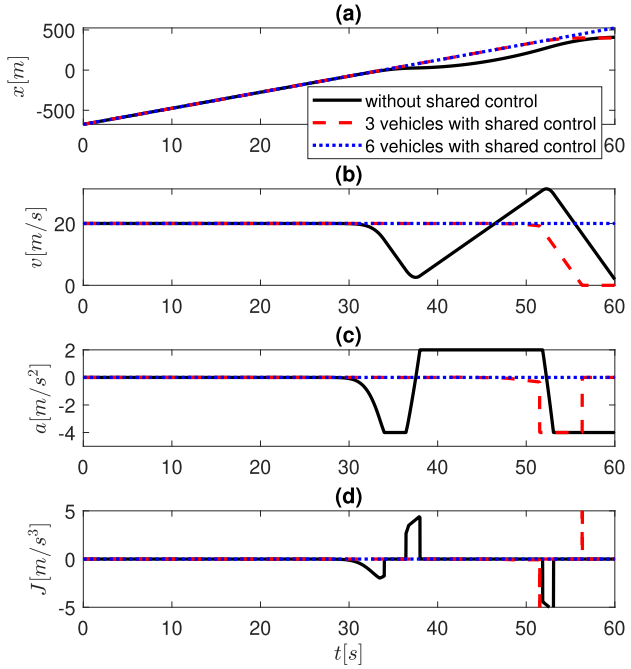

Fig. 9. Comparison of the traffic wave damping performance as a function of the number of vehicles controlled by the shared controller.

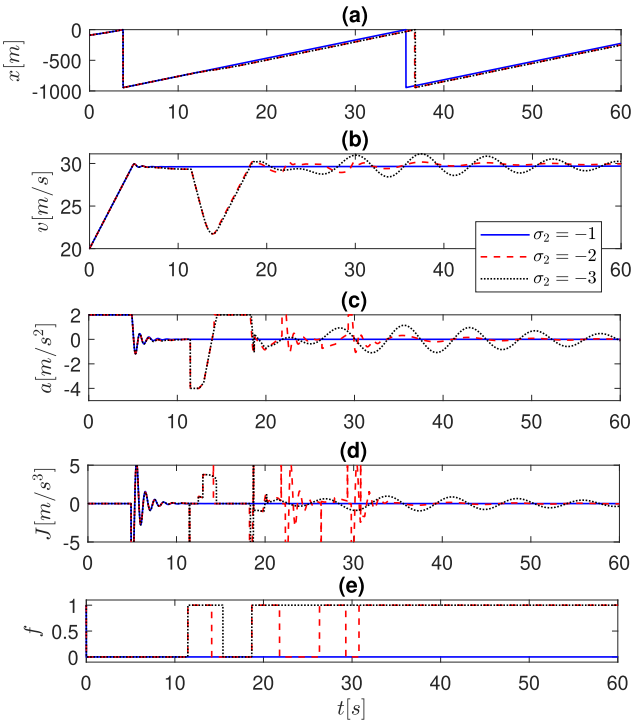

Fig. 10. Comparison of the performance as a function of σ_2.

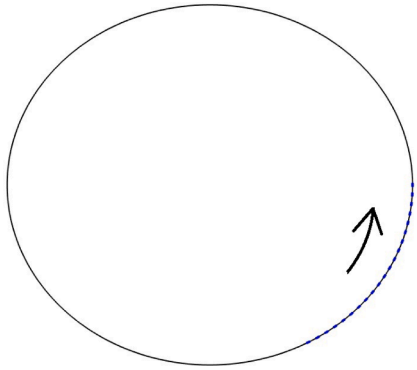

Fig. 11. Alignment of the vehicles at the beginning of the simulation. The direction of the arrow indicates the driving direction.

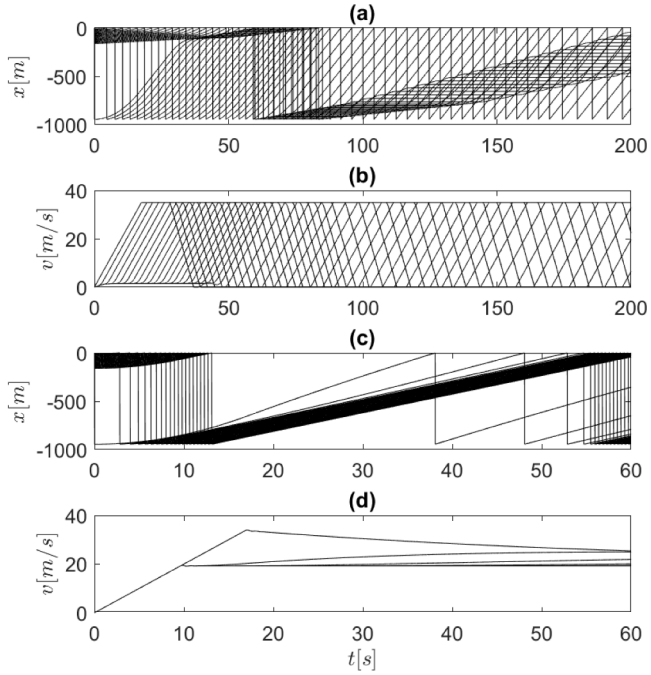

Fig. 12. Performance (*i.e.* wrapped position on the circular track, with respect to the length of the track, and speed) of all vehicles without (sub-figures (a) and (b)) and with shared control (sub-figures (c) and (d)). The received speed v^r equals the value v_i^* given in (15).

$$d_{21,1} = 785\ m \text{and} d_{i-1,i} = 8\ m,\ \forall i \in \{2, 3, \ldots, 21\}.$$

In addition, the initial speed for all vehicles are set to zero. Fig. 11 shows the distribution of the 21 vehicles at the beginning of the simulation.

Simulation results with and without the shared controller are presented in Figs. 12 and 13. Fig. 12 demonstrates that without the shared controller the speed of Vehicle 1 increases at the beginning until it reaches the maximum speed of 35 m/s. After a while, it drops to zero and the vehicle stops. However, with the shared controller, none of the vehicles stops. In addition, the speed variation has been significantly reduced to 3 m/s within 120 s. The stop-and-go wave is eliminated by the shared controller and the average traveled distances per vehicle has been increased by 23.3%, from 3650 m to 4500 m.

By comparing the simulation results shown in this subsection and the previous one, we can conclude remarkably that the proposed shared-control algorithm is beneficial regardless of the initial alignment of the vehicles.

5.4. Braking Effects Analysis

In this section we study the effects of the braking of one vehicle on the others. We assume that all vehicles are evenly distributed along the track with the same initial speed $v_i(0) = v^* = 20\ m/s$. In addition, we assume that one of the vehicles, denoted as Vehicle 1,

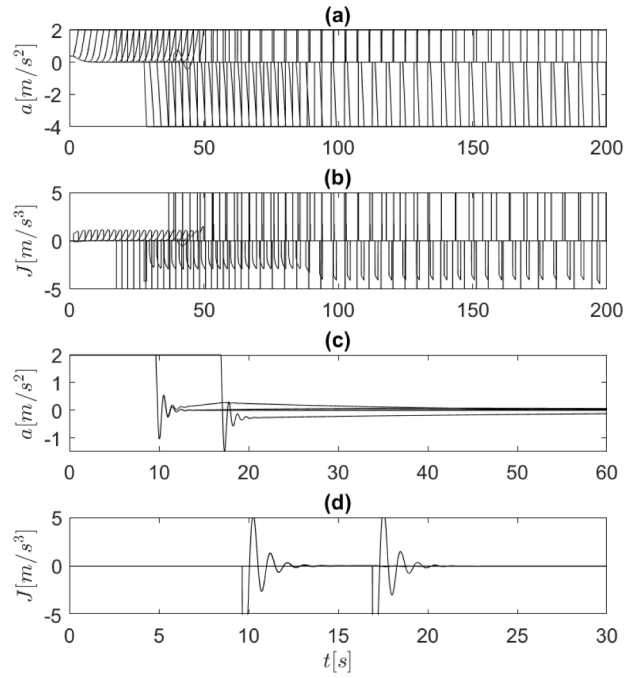

Fig. 13. Performance (*i.e.* acceleration and jerk) of all vehicles without (sub-figures (a) and (b)) and with shared control (sub-figures (c) and (d)). The received speed v^r equals the value v_i^* given in (15). Note that the jerk for the vehicles with shared control in the initial 30 *s* has been shown in sub-figures (d).

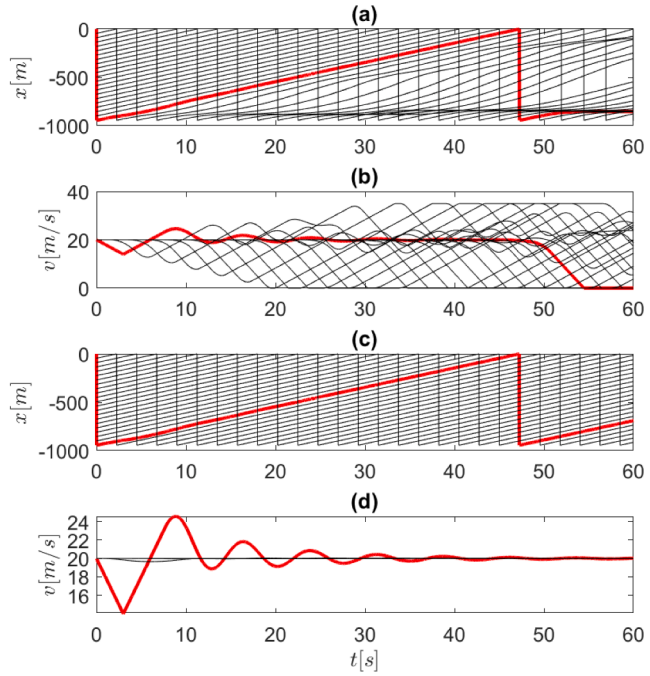

Fig. 14. Performance (*i.e.* wrapped position on the circular track, with respect to the length of the track, and speed) of all vehicles without (sub-figures (a) and (b)) and with shred control (sub-figures (c) and (d)) while Vehicle 1 brakes in the initial 3 *s*. Vehicle 1 (red solid curve) and the other 20 vehicles (black solid curve). (For interpretation of the references to colour in this figure legend, the reader is referred to the web version of this article.)

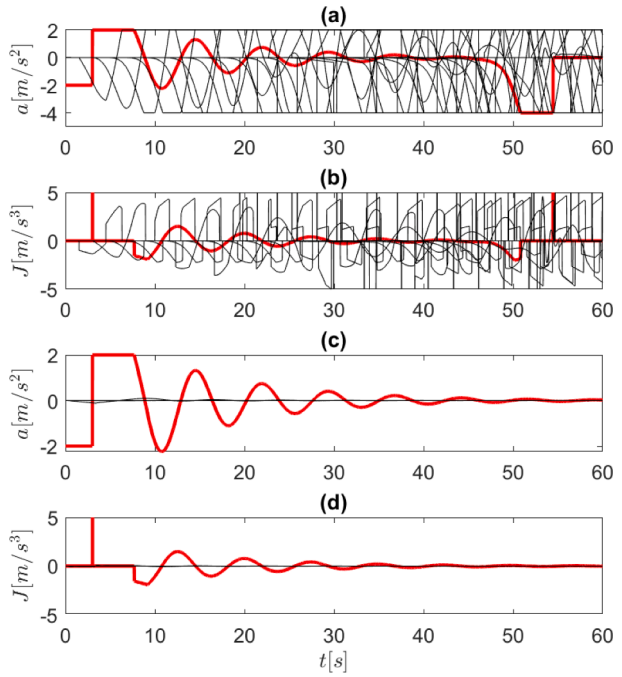

Fig. 15. Performance (*i.e.* acceleration and jerk) of all vehicles without (sub-figures (a) and (b)) and with shred control (sub-figures (c) and (d)) while Vehicle 1 brakes in the initial 3 *s*. Vehicle 1 (red solid curve) and the other 20 vehicles (black solid curve). (For interpretation of the references to colour in this figure legend, the reader is referred to the web version of this article.)

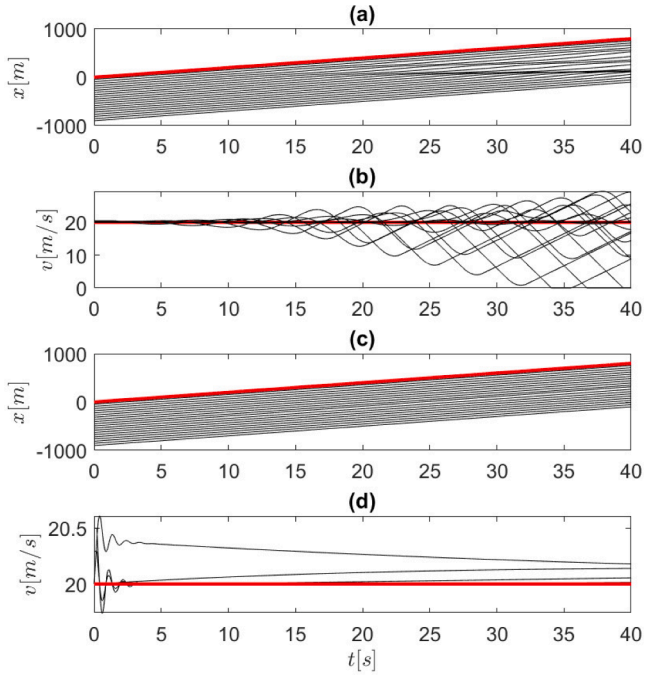

Fig. 16. Performance (*i.e.* position and speed) of all vehicles without (sub-figures (a) and (b)) and with shared control (sub-figures (c) and (d)). v^r is set to 20 m/s. Lead vehicle (*i.e.* Vehicle 1): red line, the other vehicles: black lines. (For interpretation of the references to colour in this figure legend, the reader is referred to the web version of this article.)

is controlled purely by the human driver who applies constant braking in the first 3 s, *i.e.* $a_{h1}(k) = -2\ m/s^2$ for all $k \leqslant 3/T_s$. Note that in the simulation, we randomly picked 10 vehicles controlled by the shared controller and the rest are controlled completely by the human drivers. Simulation results are shown in Figs. 14 and 15, in which the performance of all vehicles are displayed. Comparing sub-figures (a) and (b) with sub-figures (c) and (d) in Fig. 14, it is clear that the traffic has been improved with the help of the shared control as the travel distances within the same time period increase. In addition, with the use of the shared controller, the speed variations reduce and converge to less than 0.1 m/s after 40 s for all vehicles, while the speed variations achieve its maximum range (*i.e.* between zero and 35 m/s) after 30 s if there is no shared control implemented. Fig. 15 shows time histories of the acceleration a and the jerk J for all vehicles. As seen in sub-figures (a) and (c), it is obvious that the acceleration of Vehicle i is always within the bounds $[a^i_{min}, a^i_{max}]$ and magnitude of the jerk is significantly reduced by the use of the shared controller, indicating the improved comfort. Note that the first red spikes in sub-figures (b) and (d) are created by the human driver of Vehicle 1 intentionally.

5.5. Straight Line Simulation

In this section, we study how the vehicles with the shared control behave on straight freeways. To simulate this, we set a large value of the radius for the circular track, namely R is chosen as 3000 m. The initial speed of all vehicles are set to 20 m/s corrupted by zero-mean normal distributed random noises with covariance 1. Furthermore, the initial distances between adjacent vehicles are given as

$$d_{i,i+1} = 45\ m, \forall i \in \{1, 2, \ldots, 20\}.$$

Note that Vehicle 1 is regarded as the lead vehicle and there is no other vehicles in front of it.

Simulation results are given in Figs. 16 and 17, in which the effectiveness of the shared control is demonstrated as the stop-and-go wave has been completely eliminated, and the acceleration and jerk for all vehicles converge to zero after a short time period. In addition, by comparing Fig. 16 (a) and (c), we can conclude that with the use of the shared control, the number of vehicles that have passed $x = 400\ m$ within 20 s, since the lead vehicle passed it, increases from 7 to 9, indicating a 28.6% increase of flow rate.

5.6. Analysis of Areas where Recommended Traffic Speed Changes Suddenly

In this section, we study the effects of a sudden change of v^r on the behaviour of the vehicles. Note that the setup of the system is the same as that in Section 5.5: $R = 3000\ m$. However, M is chosen as 10 in this case.

We assume that the initial speeds of all vehicles are set to 30 m/s and are corrupted by zero-mean normal distributed random noise with variance 1. The initial distance are set to

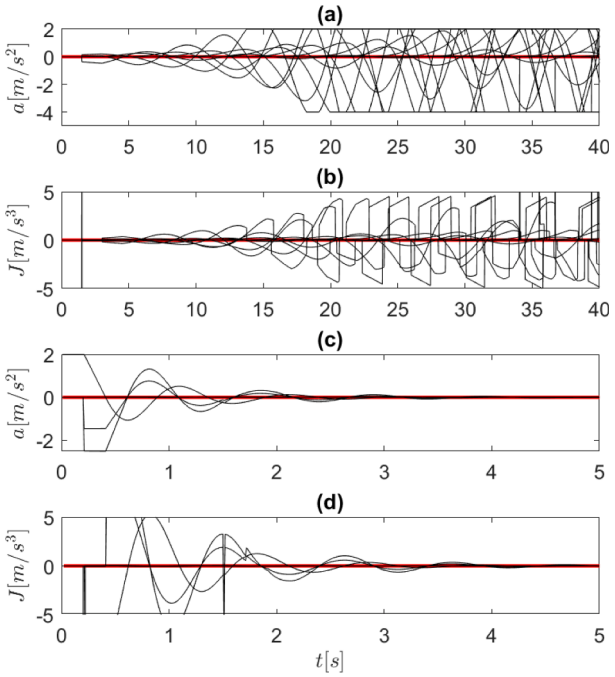

Fig. 17. Performance (*i.e.* acceleration and jerk) of all vehicles without (sub-figures (a) and (b)) and with shared control (sub-figures (c) and (d)). v^r is set to 20 m/s. Lead vehicle (*i.e.* Vehicle 1): red line, the other vehicles: black lines. The vehicle acceleration and jerk performance in the initial 5 s have been shown in sub-figures (c) and (d). (For interpretation of the references to colour in this figure legend, the reader is referred to the web version of this article.)

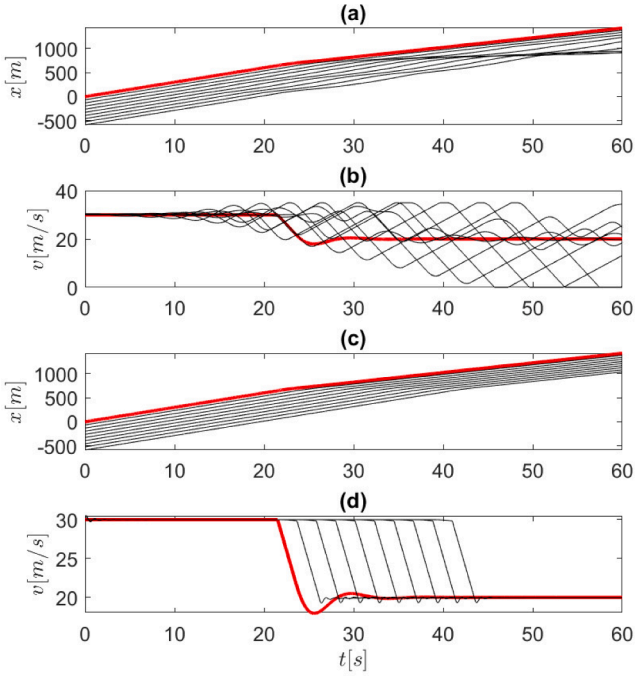

Fig. 18. Performance (*i.e.*position and speed) of all vehicles without (sub-figures (a) and (b)) and with shared control (sub-figures (c) and (d)) when v^r drops down from 30 m/s to 20 m/s suddenly. Lead vehicle (*i.e.* Vehicle 1): red line, the other vehicles: black lines. (For interpretation of the references to colour in this figure legend, the reader is referred to the web version of this article.)

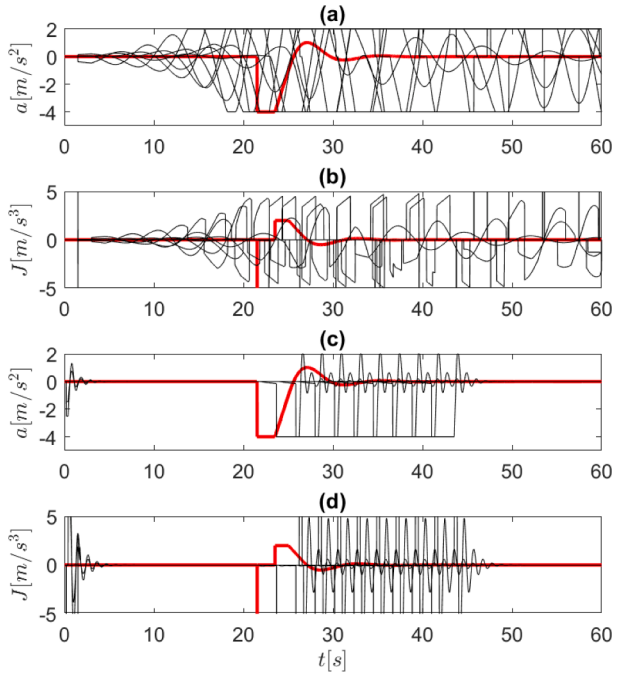

Fig. 19. Performance (*i.e.*position and speed) of all vehicles without (sub-figures (a) and (b)) and with shared control (sub-figures (c) and (d)) when v^r drops down from 30 m/s to 20 m/s suddenly. Lead vehicle (*i.e.* Vehicle 1): red line, the other vehicles: black lines. (For interpretation of the references to colour in this figure legend, the reader is referred to the web version of this article.)

$$d_{i,i+1} = 65\ m, \forall i \in \{1, 2, \ldots, 20\}.$$

We assume that v^r is given as

$$v^r = \begin{cases} 30, & \text{if } x \leqslant 600, \\ 20, & \text{otherwise.} \end{cases}$$

Simulation results are given in Figs. 18 and 19, from which we see that the speed of the vehicles starts to decrease when the position is over 600 m, *i.e.* the recommended speed v^r suddenly drops from 30 m/s to 20 m/s. As shown in Fig. 18 (b) and (d), although the lead vehicle (Vehicle 1) behaves the same, some vehicles stops after 42s without the use of the shared control. However, by the use of the shared control, each vehicle's speed drops smoothly to 20 m/s within 10 s after it enters the high-capacity zone where v^r decreases. The acceleration and jerk performance are also much improved. Note that the jerk of all vehicles converge to 0 within 10 s after the sudden decrease of v^r, while the oscillation in Fig. 19 (c) and (d) refers to behaviour of 9 different vehicles when they approach the high-capacity zone.

5.7. Simulation Robustness Analysis

In this section the robustness of the shared controller is studied. Assume that the correct suggested speed v^r equals 20 m/s. However, due to disturbances, Vehicle 1 receives $\widetilde{v}^r(k) = v^r(k) + \delta_1(k)$ with

$$\delta_1(k) = -3, \ \forall k \in \{1, 2, \ldots, \}, \tag{16}$$

and

$$\delta_1(k) = 5\sin(0.001k), \ \forall k \in \{1, 2, \ldots, \}, \tag{17}$$

representing a constant disturbance and a time-varying disturbance, respectively.

Simulation results in the presence of these two disturbances are displayed in Fig. 20-(a)-(b) and Fig. 20-(c)-(d), respectively. Note that only the responses of Vehicles 1 and 2 have been shown because all other vehicles have similar response to that of Vehicle 2. If the disturbance is a sufficiently large constant negative value, such as -3 m/s in the simulation, the control authority of Vehicle 1 is always held by the human driver (*i.e.* $f_i(k) = 1$ for all $k \in \{1, 2, \ldots, \}$) because the attacked suggested speed they receives is always smaller than the speed of the preceding vehicle, while the control authority of all the other vehicles are dynamically located between the human driver and the feedback controller. However, in the case in which the attack is defined by (17) the control authority of Vehicle 1 is not held continuously by the human driver, as shown in Fig. 20-(d), because there are time instants kT_s when the vehicle receives a much larger value of $v^r(kT_s - T_c)$ than the speed of its preceding vehicle $v_{21}(kT_s - T_d)$.

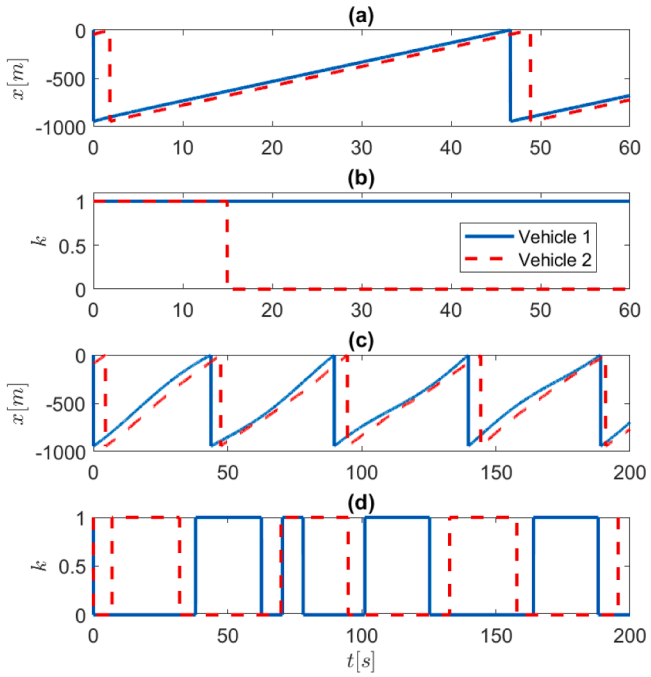

Fig. 20. Locations and allocation of control authorities for Vehicles 1 (blue, solid) and 2 (red, dashed) with a constant attack ((a) and (b)) and a time-varying attack ((c) and (d)) on Vehicle 1. (For interpretation of the references to colour in this figure legend, the reader is referred to the web version of this article.)

6. Concluding remarks

We have solved the traffic wave damping problem for vehicles on a circular track with single lane. The solution takes a model of the human behaviour into consideration and it is in line with the human driver's driving habits. We have rigorously proved that, with the car-following model of Section 2.2, the established controller is able to eliminate the stop-and-go wave, no matter how the vehicles are aligned at the beginning and what the initial speeds are. More importantly, we have proved formally that such shared-control is robust to disturbances which has important practical significance. Simulation results have been provided to show the effectiveness of the shared controller in various situations.

To investigate the perception of human drivers for this assistive function, experimental tests with various groups of users will be conducted in the future. In addition, we will devote our efforts to the development of shared control laws for systems with vehicles on road segments with multiple lanes and intersections. Such simulation setup allows lane-changing manoeuvers, external disturbances (such as in merging manoeuvers), and allows vehicles to travel in and out of the system. Future research efforts will also be devoted for formulate and solve an optimal shared-control problem in order to improve the comfort of human drivers and reduce jerks.

References

The Official DVSA Theory Test for Car Drivers. British Driver and Vehicle Standard Agency, 2016.

Abbink, D.A., Carlson, T., Mulder, M., Winter, J.C.F., Aminravan, F., Gibo, T.L., Boer, E.R., 2018. A topology of shared control systems - finding common ground in diversity. IEEE Trans on Human-Machine Systems 48 (5).

S. Ahn and M. Cassidy. Freeway traffic oscillations and vehicle lane-change maneuvers. In Proc. of Transportation and Traffic Theory, pages 691–710, 2007.

Barth, M., Boriboonsomsin, K., 2008. Real-world carbon dioxide impacts of traffic congestion. Transportation Research Record: Journal of the Transportation Research Board 2058, 163–171.

August 02) Bartlett, J.S. (2018. Best and worst car acceleration. In Retrieved from https://www.consumerreports.org/cars-best-and-worst-car-acceleration.

Brackstone, M., McDonald, M., 1999. Car-following: A historical review. Transportation Research Part F: Traffic Psychology and Behaviour 2 (4), 181–196.

Carlson, R.C., Papamichail, I., Papageorgiou, M., 2011. Local feedback-based mainstream traffic flow control on motorways using variable speed limits. IEEE Trans. on Intelligent Transportation Systems 12 (4), 1261–1276.

Carlson, R.C., Papamichail, I., Papageorgiou, M., 2014. Integrated feedback ramp metering and mainstream traffic flow control on motorways using variable speed limits. Transportation Research Part C: Emerging Technologies 46, 209–221.

Carlson, R.C., Papamichail, I., Papageorgiou, M., Messmer, A., 2010. Optimal motorway traffic flow control involving variable speed limits and ramp metering. Transportation Science 44 (2), 238–253.

Daganzo, C.F., 1994. The cell transmission model: A dynamic representation of highway traffic consistent with the hydrodynamic theory. Transportation Research Part B: Methodological 28 (4), 269–287.

C. Fabritiis, R. Ragona, and G. Valenti. Traffic estimation and prediction based on real time floating car data. In Proc. of IEEE Conference on Intelligent Transportation Systems, pages 197–203, Beijing, China, 2008.

Flynn, M.R., Kasimov, A.R., Nave, J.C., Rosales, R.R., Seibold, B., 2009. Congestion redux. SIAM Journal on Applied Mathematics 64 (4), 1175–1185.

Flynn, M.R., Kasimov, A.R., Nave, J.C., Rosales, R.R., Seibold, B., 2009. Self-sustained nonlinear waves in traffic flow. Phys. Rev. E 79 (5), 056113.

Gipps, P.G., 1981. A behavioural car-following model for computer simulation. Transportation Research Part B: Methodological 15 (2), 105–111.

Gomes, G., Horowitz, R., 2006. Optimal freeway ramp metering using the asymmetric cell transmission model. Transportation Research Part C: Emerging Technologies 14 (4), 244–262.

Greibe, P., 2007. Braking distance, friction and behaviour. Trafitec.

Guo, G., Li, D., 2019. Adaptive sliding mode control of vehicular platoons with prescribed tracking performance. IEEE Trans on Vehicular Technology 68 (8), 7511–7520.

Guo, G., Li, D., 2019. Communication scheduling and control of a platoon of vehicles in vanets. IEEE Trans on Intelligent Transportation Systems 17 (6), 1551–1563.

Guo, G., Wang, Q., 2019. Fuel-efficient en route speed planning and tracking control of truck platoons. IEEE Trans on Intelligent Transportation Systems 20 (8), 3091–3103.

A. Hegyi, S.P. Hoogendoorn, M. Schreuder, H. Stoelhorst, and F. Viti. SPECIALIST: A dynamic speed limit control algorithm based on shock wave theory. In Proc. of IEEE Conference on Intelligent Transportation Systems, pages 827–832, Beijing, China, 2008.

Hegyi, A., Schutter, B., Hellendoorn, H., 2005. Model predictive control for optimal coordination of ramp metering and variable speed limits. Transportation Research Part C: Emerging Technologies 13 (3), 185–209.

W. Helly. Simulation of bottlenecks in single lane traffic flow. In Proc. of Symposium on Theory of Traffic Flow, pages 207–238, 1959.

Hou, Z., Xu, J.X., Zhong, H., 2007. Freeway traffic control using iterative learning control-based ramp metering and speed signaling. IEEE Trans. on Vehicular Technology 52 (2), 466–477.

Jiang, J., Franco, P., Astolfi, A., 2016. Shared control for the kinematic and dynamic models of a mobile robot. IEEE Trans. on Control Systems Technology 24 (6), 2112–2124.

J.A. Laval. Linking synchronized flow and kinematic wave theory. In Proc. of Traffic and Granular Flow, pages 521–526, 2005.

Laval, J.A., Daganzo, C.F., 2006. Lane-changing in traffic streams. Transportation Research Part B: Methodological 40 (3), 251–264.

Laval, J.A., Leclercq, L., 2010. A mechanism to describe the formation and propagation of stop-and-go waves in congested freeway traffic. Philosophical Transactions of the Royal Society A 368, 4519–4541.

Laval, J.A., Leclercq, L., 2010. A mechanism to describe the formation and propagation of stop-and-go waves in congested freeway traffic. Philosophical Transactions of the Royal Society A 368 (1928), 4519–4541.

Marchesini, P., Weijermars, W., 2010. The Relationship Between Road Safety and Congestion on Motorways. SWOV Institute for Road Safety Research, Leidschendam, The Netherlands.

Orosz, G., Wilson, R.E., Szalai, R., Stépán, G., 2008. Traffic jams without bottlenecks: experimental evidence for the physical mechanism of the formation of a jam. New J. Phys. 10, 033001.

Orosz, G., Wilson, R.E., Szalai, R., Stépán, G., 2009. Exciting traffic jams: nonlinear phenomena behind traffic jam formation on highways. Phys. Rev. E 80 (4), 046205.

Papageorgiou, M., Kosmatopoulos, E., Papamichail, I., 2008. Effects of variable speed limits on motorway traffic flow. Transportation Research Record: Journal of the Transportation Research Board 2047, 37–48.

Papamichail, I., Kotsialos, A., Margonis, I., Papageorgiou, M., 2010. Coordinated ramp metering for freeway networks: A model-predictive hierarchical control approach. Transportation Research Part C: Emerging Technologies 18 (3), 311–331.

Peng, G.H., Cai, X.H., Liu, C.Q., Cao, B.F., 2011. A new lattice model of traffic flow with the consideration of the driver-+s forecast effects. Phys. Lett. A 375 (22), 2153–2157.

Seiler, P., Pant, A., Hedrick, K., 2004. Disturbance propagation in vehicle strings. IEEE Trans. on Automatic. Control 49 (10), 1835–1841.

Stern, R.E., Cui, S., Monache, M.L.D., Bhadani, R., Bunting, M., Churchill, M., Hamilton, N., Haulcy, R., Pohlmann, H., Wu, F., Piccoli, B., Seibold, B., Sprinkle, J., Work, D.B., 2018. Dissipation of stop-and-go waves via control of autonomous vehicles: Field experiments. Transportation Research Part C: Emerging Technologies 89, 205–221.

Sugiyama, Y., Fukui, M., Kikuchi, M., Hasebe, K., Nakayama, A., Nishinari, K., Tadaki, S., Yukawa, S., 2008. Traffic jams without bottlenecks: experimental evidence for the physical mechanism of the formation of a jam. New J. Phys. 10 (3), 033001.

Tadaki, S., Kikuchi, M., Fukui, M., Nakayama, A., Nishinari, K., 2013. Phase transition in traffic jam experiment on a circuit. New J. Phys. 15, 103034.

Treiber, M., Kesting, A., Helbing, D., 2006. Delays, inaccuracies and anticipation in microscopic traffic models. Phys. A 360 (1), 71–88.

Wang, C., Quddus, M.A., Ison, S.G., 2009. Impact of traffic congestion on road accidents: A spatial analysis of the M25 motorway in england. Accid. Anal. Prev. 41 (4), 798–808.

Wilson, R.E., 2008. Mechanisms for spatio-temporal pattern formation in highway traffic models. Philosophical Transactions of the Royal Society A 366 (1872), 2153–2157.

H. Yeo and A. Skabardonis. Understanding stop-and-go traffic in view of asymmetric traffic theory. Transportation and Traffic Theory 2009: Golden Jubilee, pages 99–115, 2009.

Yuan, K., Knoop, V.L., Hoogendoorn, S.P., 2015. Capacity drop: Relationship between speed in congestion and the queue discharge rate. Transportation Research Record: Journal of the Transportation Research Board 2491, 72–80.